THE JOURNAL OF BIOLOGICAL CHEMISTRY
Vol. 280, No. 33, Issue of August 19, pp. 29420–29427, 2005
Printed in U.S.A.

Microtubule Regulation of *N*-Methyl-D-aspartate Receptor Channels in Neurons*

Received for publication, April 25, 2005, and in revised form, June 6, 2005
Published, JBC Papers in Press, June 23, 2005, DOI 10.1074/jbc.M504499200

Eunice Y. Yuen, Qian Jiang, Jian Feng, and Zhen Yan‡

From the Department of Physiology and Biophysics, State University of New York at Buffalo, School of Medicine and Biomedical Sciences, Buffalo, New York 14214

***N*-Methyl-D-aspartate (NMDA) receptors (NMDARs), which play a key role in synaptic plasticity, are dynamically regulated by many signaling molecules and scaffolding proteins. Although actin cytoskeleton has been implicated in regulating NMDAR stability in synaptic membrane, the role of microtubules in regulating NMDAR trafficking and function is largely unclear. Here we show that microtubule-depolymerizing agents inhibited NMDA receptor-mediated ionic and synaptic currents in cortical pyramidal neurons. This effect was Ca^{2+}-independent, required GTP, and was more prominent in the presence of high NMDA concentrations. The NR2B subunit-containing NMDA receptor was the primary target of microtubules. The effect of microtubule depolymerizers on NMDAR currents was blocked by cellular knockdown of the kinesin motor protein KIF17, which transports NR2B-containing vesicles along microtubule in neuronal dendrites. Neuromodulators that can stabilize microtubules, such as brain-derived neurotrophic factor, significantly attenuated the microtubule depolymerizer-induced reduction of NMDAR currents. Moreover, immunocytochemical studies show that microtubule depolymerizers decreased the number of surface NR2B subunits on dendrites, which was prevented by the microtubule stabilizer. Taken together, these results suggest that interfering with microtubule assembly suppresses NMDAR function through a mechanism dependent on kinesin-based dendritic transport of NMDA receptors.**

Emerging evidence has suggested that the trafficking of NMDA[1] receptors plays a key role in regulating the function of these channels at the cell membrane (1, 2). NMDA receptors are found both in the cytoplasm of neurons and at excitatory synapses (3). After NR1 and NR2 subunits assemble together to form a functional complex, NMDA receptors overcome the endoplasmic reticulum retention and are released from the endoplasmic reticulum (4, 5). After being further processed in the cell body, NMDA receptors are rapidly transported along microtubule tracks in dendritic shafts (6), followed by the delivery to actin-rich dendritic spines.

NMDA receptors undergo regulated transport to and from the cell surface and lateral diffusion at synaptic and extrasynaptic sites in the plasma membrane (7, 8). The PDZ domain-mediated interactions between NR2 subunits and the synaptic scaffolding protein PSD-95 has been proposed to be important for stabilizing and/or promoting surface NMDA receptor expression (7, 9). Tyrosine dephosphorylation of NR1/2A receptors has also been found to be critical for triggering clathrin-dependent endocytosis (10). Moreover, NR2A and NR2B have distinct endocytic motifs and endocytic sorting, with NR2B undergoing more robust endocytosis than NR2A in mature cultures (11). Despite these findings on NMDA receptor trafficking at synapses, much remains unknown about the factors regulating the long range transport of NMDA receptors along microtubules in dendrites.

Microtubules, a polymer of α- and β-tubulins, are highly dynamic structures (12), serving as rails along which cargoes can be transported (13). They have been implicated in regulating nerve growth and dendrite formation (14, 15). Biochemical studies have identified the dynamic interaction between tubulin and C-terminal domains of NMDAR subunits (16). One class of microtubule-binding proteins that bind to tubulin polymers and regulate microtubule functions is motor proteins (kinesins and dyneins). They mediate anterograde and retrograde intracellular transport of membranous organelles, vesicles, and protein complexes along microtubules (13, 17). Biochemical and immunocytochemical studies have shown that the kinesin motor protein KIF17 is linked to NR2B-containing vesicles via a scaffolding protein complex (18) and involved in the dendritic transport of NMDA receptors (19). Because of the lack of functional studies showing the interaction between microtubule/KIF17 and NMDA receptors, we have used electrophysiological approaches to examine whether NMDA receptor-mediated currents are affected by interfering with microtubule stability and the function of motor protein KIF17.

EXPERIMENTAL PROCEDURES

Acute Dissociation Procedure—Prefrontal cortical neurons from young adult (3–4-week-postnatal) rats were acutely dissociated using procedures similar to those described previously (20, 21). All experiments were carried out with the approval of the State University of New York at Buffalo Animal Care Committee. After incubation of brain slices in a $NaHCO_3$-buffered saline, prefrontal cortex was dissected and placed in an oxygenated chamber containing papain (0.8 mg/ml; Sigma) in HEPES-buffered Hanks' balanced salt solution (Sigma) at room temperature. After 40 min of enzyme digestion, tissue was rinsed three times in the low Ca^{2+}, HEPES-buffered saline and mechanically dissociated with a graded series of fire-polished Pasteur pipettes. The cell suspension was then plated into a 35-mm Lux Petri dish, which was then placed on the stage of a Nikon inverted microscope.

Primary Neuronal Culture—Rat prefrontal cortex cultures were prepared by a modification of previously described methods (22). Briefly,

* This work was supported by grants from the National Institutes of Health (to Z. Y. and J. F.). The costs of publication of this article were defrayed in part by the payment of page charges. This article must therefore be hereby marked "*advertisement*" in accordance with 18 U.S.C. Section 1734 solely to indicate this fact.

‡ To whom correspondence should be addressed: Dept. of Physiology and Biophysics, State University of New York at Buffalo, 124 Sherman Hall, Buffalo, NY 14214. E-mail: zhenyan@buffalo.edu.

[1] The abbreviations used are: NMDA, *N*-methyl-D-aspartate; EPSC, excitatory postsynaptic current; ANOVA, analysis of variance; NMDAR, NMDA receptor; PFC, prefrontal cortex; BAPTA, 1,2-bis(2-aminophenoxy)ethane-*N*,*N*,*N*′,*N*′-tetraacetic acid; GFP, green fluorescent protein; MAP, microtubule-associated protein; MES, 4-morpholinoethanesulfonic acid; BDNF, brain-derived neurotrophic factor.

prefrontal cortex was dissected from 18-day rat embryos, and cells were dissociated using trypsin and trituration through a Pasteur pipette. The neurons were plated on coverslips coated with poly-L-lysine in Dulbecco's modified Eagle's medium with 10% fetal calf serum at a density of 3000 cells/cm^2. When neurons attached to the coverslip within 24 h, the medium was changed to Neurobasal with B27 supplement. Neurons were maintained for 3 weeks before being used for recordings.

Whole Cell Recordings—Whole cell recordings of whole cell ion channel currents employed standard voltage clamp techniques (22, 23). The internal solution consisted of 180 mM *N*-methyl-D-glucamine, 40 mM HEPES, 4 mM $MgCl_2$, 0.1 mM BAPTA, 12 mM phosphocreatine, 3 mM Na_2ATP, 0.5 mM Na_2GTP, 0.1 mM leupeptin, pH 7.2–7.3, 265–270 mosM. The external solution consisted of 127 mM NaCl, 20 mM CsCl, 10 mM HEPES, 1 mM $CaCl_2$, 5 mM $BaCl_2$, 12 mM glucose, 0.001 mM tetrodotoxin (TTX), 0.02 mM glycine, pH 7.3–7.4, 300–305 mosM. Recordings were obtained with an Axon Instruments 200B patch clamp amplifier that was controlled and monitored with an IBM PC running pCLAMP (version 8) with a DigiData 1320 series interface (Axon instruments). Electrode resistances were typically 2–4 megaohms in the bath. After seal rupture, series resistance (4–10 megaohms) was compensated (70–90%) and periodically monitored. The cell membrane potential was held at −60 mV. The application of NMDA (100 μM) evoked a partially desensitizing inward current that could be blocked by the NMDA receptor antagonist D-2-amino-5-phosphonovaleric acid (50 μM). NMDA was applied for 2 s every 30 s to minimize desensitization-induced decrease of current amplitude. Drugs were applied with a gravity-fed "sewer pipe" system. The array of application capillaries (~150-μm inner diameter) was positioned a few hundred μm from the cell under study. Solution changes were effected by the SF-77B fast step solution stimulus delivery device (Warner Instruments).

Data analyses were performed with AxoGraph (Axon instruments), Kaleidagraph (Albeck Software), Origin 6 (OriginLab), and Statview (Abacus Concepts). For analysis of statistical significance, Mann-Whitney U tests were performed to compare the current amplitudes in the presence or absence of various agents. ANOVA tests were performed to compare the differential degrees of current modulation between groups subjected to different treatment. The dose-response data were fitted with the equation, $Y = Y_0/(1 + (C/\tau)^S)$, where C represents the concentration, τ is the EC_{50}, and S is the slope factor.

Electrophysiological Recordings in Slices—To evaluate the regulation of NMDAR-mediated excitatory postsynaptic currents by microtubules in prefrontal cortex (PFC) slices, the whole cell voltage clamp recording technique was used (22). Electrodes (5–9 megaohms) were filled with the following internal solution: 130 mM Cs-methanesulfonate, 10 mM CsCl, 4 mM NaCl, 10 mM HEPES, 1 mM $MgCl_2$, 5 mM EGTA, 2.2 mM QX-314, 12 mM phosphocreatine, 5 mM MgATP, 0.2 mM Na_3GTP, 0.1 mM leupeptin, pH 7.2–7.3, 265–270 mosM. The slice (300 μm) was placed in a perfusion chamber attached to the fixed stage of an upright microscope (Olympus) and submerged in continuously flowing oxygenated artificial cerebrospinal fluid. Cells were visualized with a ×40 water immersion lens and illuminated with near IR light, and the image was detected with an IR-sensitive CCD camera. A Multiclamp 700A amplifier was used for these recordings. Tight seals (2–10 gigaohms) from visualized pyramidal neurons were obtained by applying negative pressure. The membrane was disrupted with additional suction, and the whole cell configuration was obtained. The access resistances ranged from 13–18 megaohms and were compensated 50–70%. For the recording of NMDAR-mediated EPSCs, cells were bathed in artificial cerebrospinal fluid containing 6-cyano-7-nitroquinoxaline-2,3-dione (CNQX) (20 μM) and bicuculline (10 μM) to block α-amino-3-hydroxy-5-methyl-4-isoxazolepropionic acid/kainate receptors and $GABA_A$ receptors. Evoked currents were generated with a 50-μs pulse from a stimulation isolation unit controlled by a S48 pulse generator (Astro-Med). A bipolar stimulating electrode (Fredrick Haer Company, Bowdoinham, ME) was positioned ~100 μm from the neuron under recording. Before stimulation, cells (voltage-clamped at −70 mV) were depolarized to +60 mV for 3 s to fully relieve the voltage-dependent Mg^{2+} block of NMDAR channels. The Clampfit program (Axon Instruments) was used to analyze evoked synaptic activity. The amplitude of EPSC was calculated by taking the mean of a 2–4-ms window around the peak and comparing with the mean of a 4–8-ms window immediately before the stimulation artifact.

Antisense—To knock down the expression of KIF17 in cultured cortical neurons, we used the antisense oligonucleotide approach as previously described (19). The antisense oligonucleotide against KIF17 cDNA was 5′-CAGAGGCTCACCACCGAA-3′, and the corresponding sense oligonucleotide was 5′-TTCGGTGGTGAGCCTCTG-3′. After 8–11 days of culture, 1 μM oligonucleotides was added directly to the culture medium. 2–3 days after being exposed to these oligonucleotides, electrophysiological recordings were performed on the cultured neurons.

Determination of Microtubule Stability—Free tubulin was extracted as previously described (24). Cultured cortical neurons (14 days *in vitro*) in 3.5-cm dishes were washed twice with 1 ml of microtubule-stabilizing buffer (0.1 M MES (pH 6.75), 1 mM $MgSO_4$, 2 mM EGTA, 0.1 mM EDTA, 4 M glycerol). Cells were then incubated at 37 °C for 5 min in 600 μl of soluble tubulin extraction buffer (0.1 M MES (pH 6.75), 1 mM $MgSO_4$, 2 mM EGTA, 0.1 mM EDTA, 4 M glycerol, 0.1% Triton X-100) with the addition of protease inhibitor mixture tablets (Roche Applied Science). The soluble extract was centrifuged at 37 °C for 2 min, and the supernatant was saved. An equal amount of protein was separated by a 10% SDS-polyacrylamide gel. Western blot was performed using anti-α-tubulin (1:2000; Sigma) as the primary antibody. After Western blot, the tubulin bands were scanned and quantitatively analyzed with NIH Image.

Immunocytochemical Staining—For the detection of GFP-NR2B (25) on the cell surface, cultured neurons were treated with different agents following transfection, and then they were fixed in 4% paraformaldehyde but not permeabilized. After background blocking in bovine serum albumin, the cells were incubated with the anti-GFP antibody (1:100; Chemicon) at room temperature for 1 h. After washing off the primary antibodies, the cells were incubated with a rhodamine-conjugated secondary antibody (1:200; Sigma) for 50 min at room temperature. After washing in phosphate-buffered saline three times, the coverslips were mounted on slides with VECTASHIELD mounting medium (Vector Laboratories). Fluorescent images were obtained using a ×60 objective with a cooled CCD camera mounted on a Nikon microscope.

The surface GFP-NR2B clusters were measured using the Image J software. All specimens were imaged under identical conditions and analyzed using identical parameters. To define dendritic clusters, a single threshold was chosen manually, so that clusters corresponded to puncta of 2-fold greater intensity than the diffuse fluorescence on the dendritic shaft. 3–4 independent experiments for each of the treatments were performed. On each coverslip, the cluster density, size, and fluorescence intensity of 4–6 neurons (2–3 dendritic segments of at least 50 μm length per neuron) were measured. Quantitative analyses were conducted blindly (without knowledge of experimental treatment).

RESULTS

Depolymerizing Microtubule Causes a Potent Reduction of NMDAR Currents—To test the hypothesis that interference of NMDA receptor transport along microtubules in dendrites could affect NMDAR currents, we examined the effect of agents that depolymerize microtubules on whole cell NMDAR-mediated currents in cultured or acutely dissociated pyramidal neurons from PFC. As shown in Fig. 1, *A* and *B*, application of the microtubule-depolymerizing agent nocodazole (30 μM) caused a gradual decline of NMDAR currents. This effect had slow onset kinetics, taking 10–20 min to stabilize. Colchicine (30 μM), another microtubule-depolymerizing agent, induced a similar inhibition of NMDAR currents (Fig. 1*C*). Without these agents, the amplitude of NMDAR currents was stable throughout the recording (Fig. 1, *A* and *C*). As summarized in Fig. 1*D*, in a sample of cultured PFC pyramidal neurons we tested, both nocodazole and colchicine significantly reduced NMDAR currents (nocodazole: 27.1 ± 1.5%, $n = 38$; colchicine: 29.0 ± 2.8%, $n = 5$; $p < 0.001$, Mann-Whitney). Similar effects were found in acutely dissociated neurons we tested (nocodazole: 22.6 ± 1.4%, $n = 19$; colchicine: 19.4 ± 1.5%, $n = 19$; $p < 0.001$, Mann-Whitney).

Because the NMDA-evoked current in isolated neurons is mediated by both synaptic and extrasynaptic NMDA receptors, we further examined the effect of microtubule-depolymerizing agents on NMDAR-EPSCs evoked by stimulation of synaptic NMDA receptors in PFC slices. As shown in Fig. 1, *E* and *F*, application of colchicine (30 μM) induced a significant reduction in the amplitude of NMDAR-EPSCs. In parallel control measurements, NMDAR-EPSCs remained stable throughout the recording. In a sample of PFC pyramidal neurons we examined,

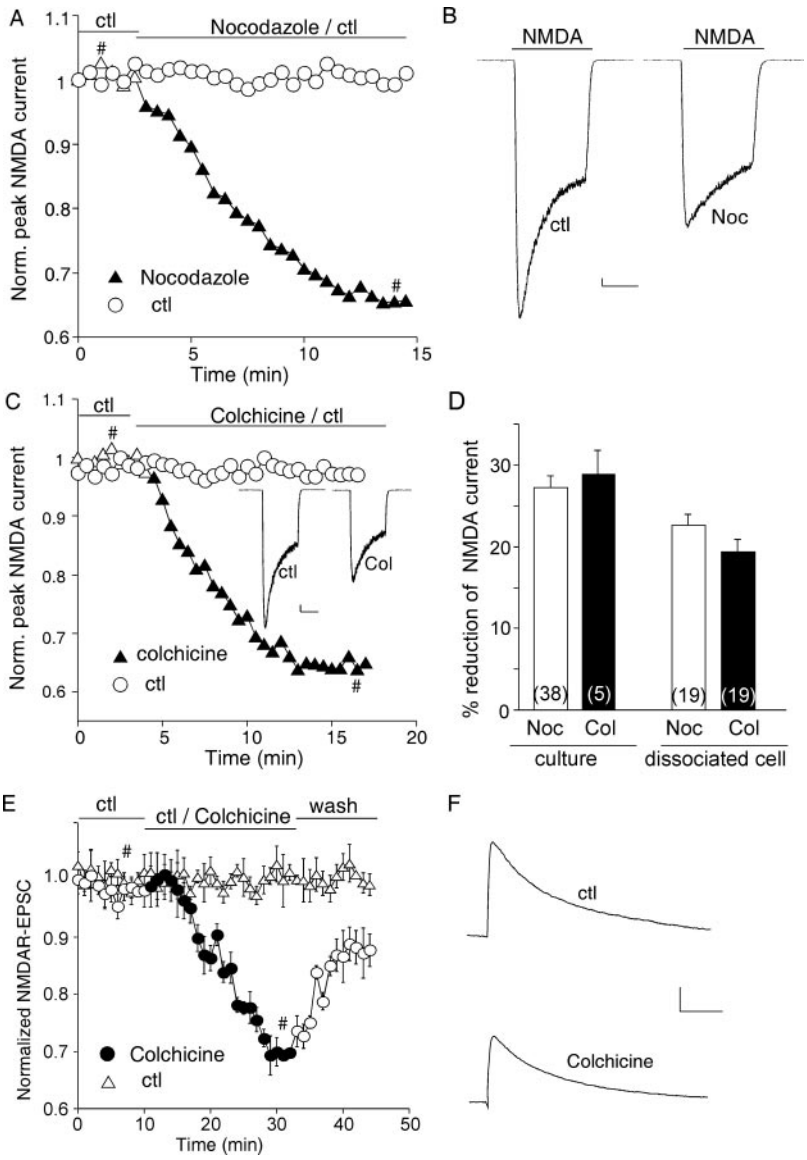

FIG. 1. **Application of microtubule depolymerizers reduced NMDAR-mediated currents.** *A* and *C*, plot of normalized peak NMDAR currents showing that the microtubule-depolymerizing agent nocodazole (*Noc*; 30 μM) (*A*) or colchicine (30 μM (*C*) decreased NMDA (100 μM)-evoked currents in cultured PFC pyramidal neurons. *B*, representative current traces taken from the records used to construct *A* (at time points denoted by #). *Inset* (*C*), representative current traces (at time points denoted by #). *Scale bars*, 100 pA, 1 s. *D*, cumulative data (mean ± S.E.) showing the percentage reduction of NMDAR currents by nocodazole or colchicine in a sample of cultured or acutely dissociated neurons. The number of cells tested is shown in *parentheses*. *E*, plot of normalized peak evoked NMDAR-EPSCs in pyramidal neurons from PFC slices with or without exposure to colchicine (30 μM). Each point represents the average peak (mean ± S.E.) of three consecutive NMDAR-EPSCs. *F*, representative current traces (average of 10 trials) taken from the records used to construct *E* (at time points denoted by #). *Scale bars*, 100 pA, 100 ms. *ctl*, control.

colchicine decreased the mean amplitude of NMDAR-EPSCs by 33.1 ± 3.3% ($n = 7$, $p < 0.001$, Mann-Whitney).

To confirm the microtubule dependence of the effect of nocodazole or colchicine on NMDAR currents, we applied taxol, a microtubule-stabilizing agent. As shown in Fig. 2, *A* and *B*, bath application of taxol (10 μM) caused little change on NMDAR currents, but it abolished the effect of nocodazole or colchicine on NMDAR currents. Washing off taxol led to the recovery of the inhibitory effect of nocodazole or colchicine. Similarly, intracellular injection of taxol (40 μM) also blocked the effect of nocodazole on NMDAR currents (Fig. 2*C*). As summarized in Fig. 2*D*, in the presence of taxol, the effect of nocodazole or colchicine on NMDAR currents was significantly attenuated (nocodazole: 22.8 ± 3.4%, $n = 6$; nocodazole + taxol: 2.2 ± 1.0%, $n = 6$; $p < 0.005$, ANOVA; colchicine: 21 ± 1.7%, $n = 6$; colchicine + taxol: 5.9 ± 1.4%, $n = 6$; $p < 0.005$, ANOVA). Taxol itself had little effect on NMDAR currents (4.8 ± 0.9%, $n = 13$; $p > 0.05$, Mann-Whitney).

The Microtubule Regulation of NMDAR Currents Is Ca^{2+}-independent but Depends on GTP and the Concentration of NMDA—Previous studies have shown that NMDA receptors are affected by the integrity of F-actin (26). Thus, we compared the effect of actin or microtubule depolymerizing agents on NMDAR currents. As shown in Fig. 3*A*, application of the potent actin depolymerizer latrunculin B (5 μM) resulted in a gradual decrease of NMDAR current, similar to the effect of microtubule-depolymerizing agents (Fig. 1). However, when cells were injected with a high concentration of BAPTA (10 mM) to prevent the elevation of intracellular Ca^{2+}, latrunculin B lost the capability to inhibit NMDAR currents, whereas the effect of nocodazole was intact (Fig. 3*B*). As summarized in Fig. 3*C*, latrunculin B and nocodazole produced a similar reduction of NMDAR currents in the absence of intracellular Ca^{2+} chelator (nocodazole: 29.8 ± 1.2%, $n = 5$; latrunculin B: 25.3 ± 2.8%, $n = 6$; $p < 0.001$, Mann-Whitney), but the effect of latrunculin B was almost abolished by high BAPTA (6.4 ± 1.1%, $n = 5$, $p > 0.05$, Mann-Whitney), whereas the effect of nocodazole was not affected by high BAPTA (28.8 ± 2.8%, $n = 4$, $p < 0.001$, Mann-Whitney). These results suggest that actin regulates NMDA receptors through a Ca^{2+}-dependent mechanism, whereas the microtubule-based regulation of NMDA receptors is Ca^{2+}-independent.

The effect of microtubule-depolymerizing agents on NMDAR currents found in this study was in contrast with the previous finding showing the lack of effect with colchicine (26). Several reasons may explain the discrepancy. First, we found that the effect of microtubule-depolymerizing agents on NMDAR currents required the presence of GTP, which plays a crucial role

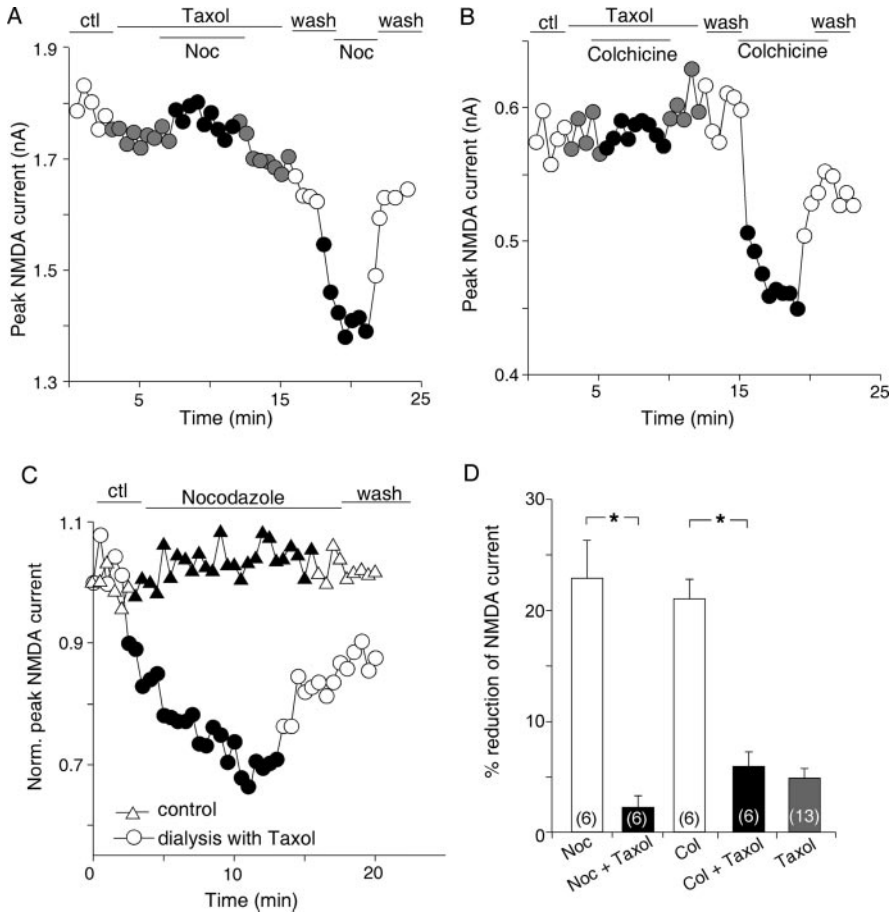

FIG. 2. **The microtubule stabilizer prevented the suppression of NMDAR currents by microtubule depolymerizers.** *A* and *B*, plot of peak NMDAR currents showing that the microtubule-stabilizing agent taxol (10 μM) blocked the effect of nocodazole (*Noc*; 30 μM) (*A*) or colchicine (30 μM) (*B*). *C*, plot of normalized peak NMDAR currents showing the effect of nocodazole in cells dialyzed with or without taxol (40 μM). *D*, cumulative data (mean ± S.E.) showing the percentage reduction of NMDAR currents by various agents. The number of cells tested is shown in *parentheses*. *, $p < 0.005$, ANOVA. *ctl*, control.

in regulating microtubule dynamics (12). When neurons were dialyzed with a GTP-free solution as previously described (26), NMDAR currents showed a fast decline, and subsequent application of nocodazole failed to produce any further effect ($n = 5$, Fig. 4*A*). Second, we found that the effect of microtubule-depolymerizing agents on NMDAR currents was dependent on the concentration of NMDA (Fig. 4*B*). When a low concentration (10 μM) of NMDA was applied to elicit NMDAR currents as previously described (26), nocodazole had little effect (2.0 ± 1.2%, $n = 5$, $p > 0.05$, Mann-Whitney), but nocodazole caused a potent reduction of the current evoked by high concentrations (100–500 μM) of NMDA (100 μM: 22.8 ± 2.5%, $n = 8$; 500 μM: 26.2 ± 2.5%, $n = 5$; $p < 0.001$, Mann-Whitney). As shown in the full concentration response curve (Fig. 4*C*), nocodazole produced a half-maximal effect at 36.6 μM NMDA. Comparing the dose responses of NMDAR currents in cells treated with or without nocodazole (Fig. 4*D*), we found that the EC_{50} was not significantly changed (nontreated: 45.5 μM; nocodazole-treated: 38.1 μM), but the current amplitude was significantly reduced by nocodazole at high concentrations of NMDA, suggesting that the surface NMDAR numbers are decreased after nocodazole treatment. These results indicate that the regulatory effect of microtubule dynamics is more prominent only when a large pool of NMDA receptors on the membrane is activated by high concentrations of NMDA.

The Microtubule Regulation of NMDAR Currents Primarily Targets NR2B-containing NMDA Receptor Channels—The primary NMDA receptors in mature cortical synapses, which are composed of NR1/NR2A or NR1/NR2B, have different subcellular localization (27, 28). NR2A-containing NMDA receptors are mainly concentrated at postsynaptic densities of dendritic spines, whereas NR2B-containing NMDA receptors are located at synaptic and extrasynaptic sites of dentritic shafts and spines (29, 30). To determine which subpopulation(s) of NMDARs is modulated by microtubules, we applied the selective inhibitor of the NR2B subunit, ifenprodil (31). Blocking NR2B subunit-containing NMDARs with ifenprodil (3 μM) reduced the amplitude of NMDAR currents by 53.3 ± 2.0% in acutely isolated PFC pyramidal neurons ($n = 14$). In the presence of ifenprodil, nocodazole had almost no effect on the remaining NMDAR currents (Fig. 5, *A* and *B*). In a sample of dissociated neurons we tested (Fig. 5*C*), ifenprodil significantly blocked the effect of nocodazole on NMDAR currents (nocodazole: 24 ± 2.5%, $n = 7$; nocodazole + ifenprodil: 2.4 ± 1.3%, $n = 8$; $p < 0.005$, ANOVA). Moreover, ifenprodil (3 μM) reduced the amplitude of NMDAR-EPSCs by 34.0 ± 2.0% in PFC pyramidal neurons from slices ($n = 6$). In the presence of ifenprodil, colchicine (30 μM) had much less effect on the remaining NMDAR-EPSCs (Fig. 5, *D–F*, colchicine: 33.1 ± 3.3%, $n = 7$; colchicine + ifenprodil: 9.3 ± 0.7%, $n = 5$; $p < 0.01$, ANOVA). These data suggest that NR2B subunit-containing NMDA receptors are the primary targets of microtubule regulation.

The Microtubule Regulation of NMDAR Currents Involves the Transport of NR2B-containing Vesicles by the Kinesin Motor Protein KIF17—KIF17, a kinesin motor protein, is linked to NR2B-containing vesicles (18). To test whether the KIF17-mediated transport of NMDA receptors is involved in the microtubule regulation of NMDAR currents, we performed cellular knockdown of KIF17 by treatment of cortical cultures with antisense oligonucleotides (1 μM) and examined the effect of nocodazole on NMDAR currents in these cultures. KIF17 sense oligonucleotides (1 μM) were used as a control. It has been shown that KIF17 antisense oligonucleotides totally inhibited KIF17 expression in hippocampal cultures (19). We found that in cultured PFC neurons treated with KIF17 antisense oligonucleotides, the basal whole cell NMDAR currents were reduced (nontreated: 1122.2 ±

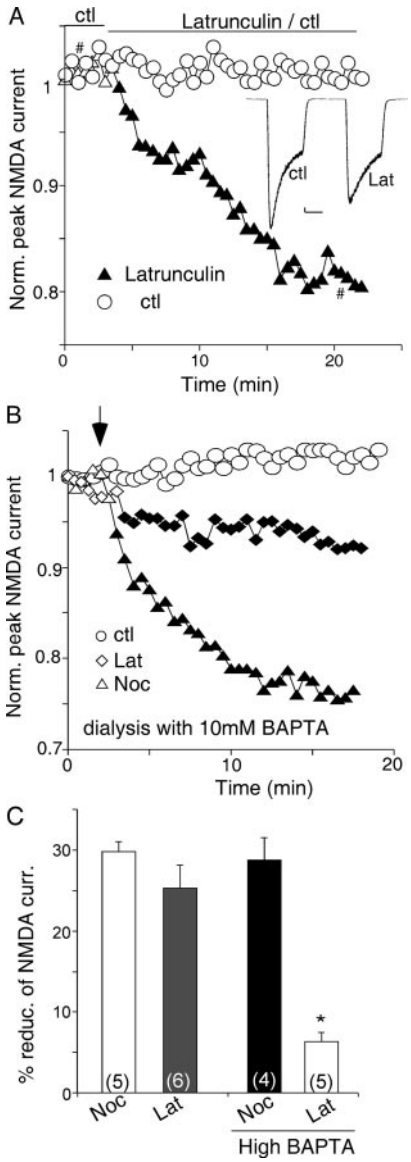

FIG. 3. **The regulation of NMDAR currents by microtubule or actin had different Ca^{2+} dependence.** *A*, plot of normalized peak NMDAR currents showing the effect of the actin-depolymerizing agent latrunculin B (*Lat*; 5 μM). *Inset*, representative current traces (at time points denoted by #). *Scale bars*, 100 pA, 1 s. *B*, plot of normalized peak NMDAR currents showing that dialysis with a high concentration of BAPTA (10 mM) blocked the effect of latrunculin B but not nocodazole (*Noc*; 30 μM). *C*, cumulative data (mean ± S.E.) showing the percentage reduction of NMDAR currents by latrunculin B or nocodazole in the absence or presence of high BAPTA. The number of cells tested is shown in *parentheses*. *, $p < 0.005$, ANOVA. *ctl*, control.

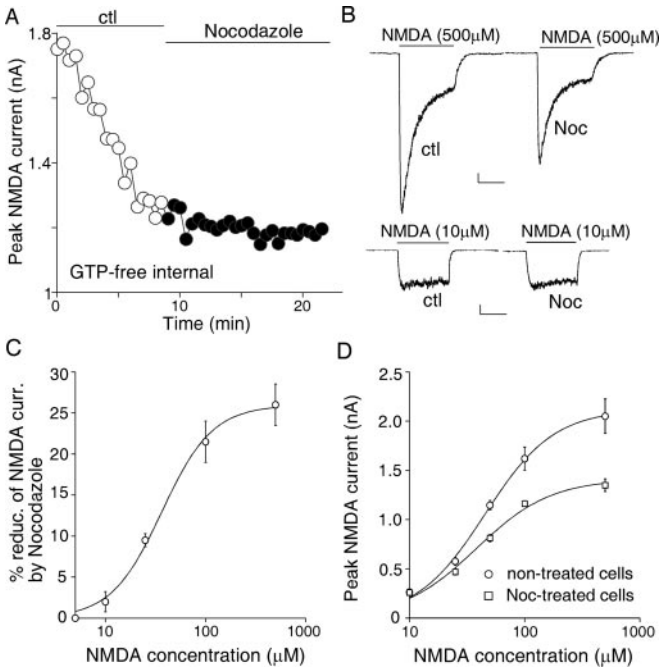

FIG. 4. **The microtubule regulation of NMDAR currents required GTP and depended on the concentration of NMDA.** *A*, plot of peak NMDA (100 μM)-evoked currents in a PFC pyramidal neuron dialyzed with the GTP-free internal solution. Note that without GTP, the current amplitude gradually declined, and subsequent application of the microtubule-depolymerizing agent nocodazole (30 μM) had no further effect on the current. *B*, representative recordings in dissociated PFC pyramidal neurons showing that nocodazole (*Noc*; 30 μM) had little effect on the current evoked by a low concentration of NMDA (10 μM) but caused a potent reduction of the current evoked by a high concentration of NMDA (500 μM). *Scale bars*, 100 pA, 1 s. *C*, full concentration response curve showing the percentage reduction by nocodazole of the current evoked by different concentrations of NMDA. Each point is the mean ± S.E. of 5–8 cells. *D*, dose-response curves of peak NMDAR currents in cells treated with ($n = 6$) or without ($n = 4$) nocodazole (30 μM, 30 min). *ctl*, control.

92.8 pA, $n = 10$; KIF antisense: 546.7 ± 36.7 pA, $n = 23$; KIF sense: 1380 ± 355.6 pA, $n = 6$), but the selective NR2B inhibitor ifenprodil (3 μM) reduced the whole cell NMDAR currents by 63.8 ± 3.5% ($n = 11$), suggesting that a significant portion of NR2B-containing channels remained in the KIF17 antisense-treated neurons. Application of nocodazole had little effect on NMDAR currents in neurons exposed to KIF17 antisense oligonucleotides, whereas the effect of nocodazole was intact in neurons exposed to KIF17 sense oligonucleotides (Fig. 6, *A* and *B*). As summarized in Fig. 6*C*, nocodazole produced little reduction of NMDAR currents in KIF17 antisense-treated neurons (3.5 ± 1.0%, $n = 13$, $p > 0.05$, Mann-Whitney), which was significantly different from the effect of nocodazole in cultured neurons treated with KIF17 sense oligonucleotides (26.6 ± 1.9%, $n = 5$, $p < 0.001$, Mann-Whitney). These results suggest that the microtubule regulation of NMDAR currents involves the transport of NR2B-containing NMDA receptors in dendrites by the motor protein KIF17.

Neurotrophins Stabilize the Microtubule Network and Prevent the Suppression of NMDAR Currents by Microtubule Depolymerizers—The electrophysiological evidence has suggested that microtubule regulates NMDAR currents through a transport-dependent mechanism; we further tested whether some neuromodulators could alter microtubule stability, leading to the change of microtubule regulation of NMDA receptors. Biochemical measurements were used to compare the level of free (depolymerized) tubulin in cultured PFC neurons subjected to treatment with nocodazole in the absence or presence of BDNF. As shown in Fig. 7, *A* and *B*, application of nocodazole (10 μM) caused a potent increase in free tubulin (2.2 ± 0.15-fold increase, $n = 3$, $p < 0.001$, ANOVA); however, this effect was significantly blocked by BDNF (20 ng/ml) treatment (0.3 ± 0.18-fold increase, $n = 3$), indicating that BDNF could increase microtubule stability and prevent nocodazole-induced microtubule depolymerization.

We then examined the effect of microtubule depolymerizers on NMDAR currents in cells treated with BDNF. As shown in Fig. 7, *C* and *D*, in the presence of BDNF (10 ng/ml), nocodazole markedly lost the capability to reduce NMDAR currents. In a sample of neurons we tested (Fig. 7*E*), nocodazole produced a little effect on NMDAR currents in neurons treated with BDNF (6.7 ± 1.4%, $n = 11$, $p > 0.05$, Mann-Whitney), which was significantly smaller than the effect of nocodazole in the absence of BDNF

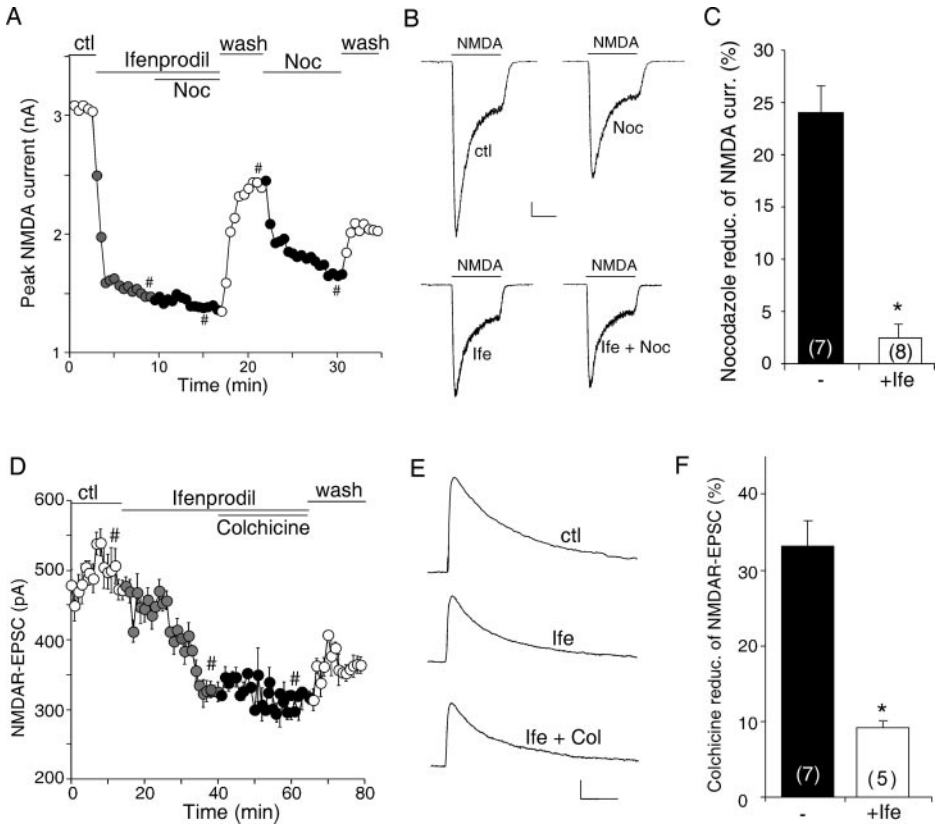

FIG. 5. **Microtubule targeted NR2B-containing NMDAR channels.** *A*, plot of peak NMDAR currents showing the effect of nocodazole (*Noc*; 30 μM) in the absence or presence of ifenprodil (3 μM), the selective inhibitor of NR2B subunit. *B*, representative current traces taken from the records used to construct *A* (at time points denoted by #). *Scale bars*, 200 pA, 1 s. *C*, cumulative data (mean ± S.E.) showing the percentage reduction of NMDAR currents by nocodazole in the absence or presence of ifenprodil (*Ife*). The number of cells tested is shown in *parentheses*. *, $p < 0.005$, ANOVA. *D*, plot of peak NMDAR-EPSCs showing the effect of colchicine (30 μM) in the presence of ifenprodil (3 μM). Each point represents the average peak (mean ± S.E.) of three consecutive NMDAR-EPSCs. *E*, representative current traces (average of 10 trials) taken from the records used to construct *D* (at time points denoted by #). *Scale bars*, 100 pA, 100 ms. *F*, cumulative data (mean ± S.E.) showing the percentage reduction of NMDAR-EPSCs by colchicine in the absence or presence of ifenprodil. The number of cells tested is shown in *parentheses*. *, $p < 0.01$, ANOVA. *ctl*, control.

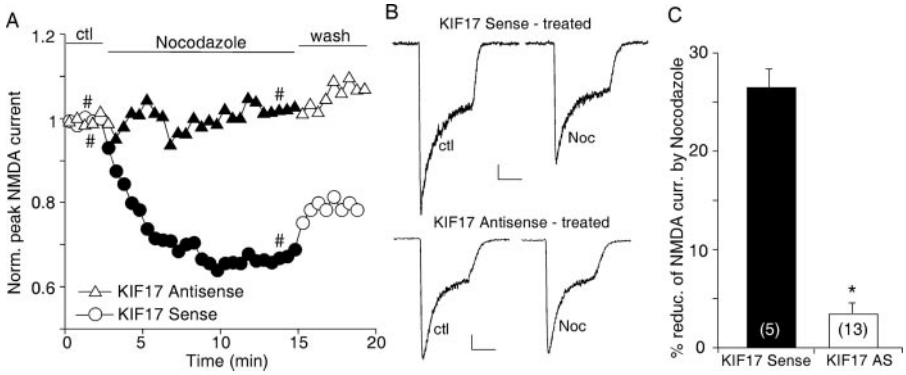

FIG. 6. **The microtubule modulation of NMDAR currents involved the transport of NR2B-containing vesicles by the kinesin motor protein KIF17.** *A*, plot of normalized peak NMDAR currents showing the effect of nocodazole (30 μM) in neurons treated with KIF17 antisense or sense oligonucleotides. *B*, representative current traces taken from the records used to construct *A* (at time points denoted by #). *Scale bars*, 100 pA, 1 s. *C*, cumulative data (mean ± S.E.) showing the percentage reduction of NMDAR currents by nocodazole in a sample of cultured neurons treated with KIF17 antisense (*AS*) or sense oligonucleotides. The number of cells tested is shown in *parentheses*. *, $p < 0.005$, ANOVA. *ctl*, control; *Noc*, nocodazole.

(22.7 ± 2.0%, $n = 7$, $p < 0.001$, Mann-Whitney). To test whether BDNF treatment alone may increase NMDAR currents and is simply offsetting the effect of nocodazole, we also examined the effect of BDNF on NMDAR currents. As shown in Fig. 7*F*, bath application of BDNF (10 ng/ml) had little effect on NMDAR currents (2.3 ± 1.4%, $n = 4$, $p > 0.05$, Mann-Whitney). These data suggest that the microtubule regulation of NMDA receptors can be altered by neuromodulators that are capable of affecting the stability of the microtubule network.

Microtubule Depolymerizers Reduce the Number of Surface NR2B Subunits on Neuronal Dendrites—To provide morphological evidence of the changes of NMDAR distribution induced by microtubule depolymerizers, we performed the quantitative surface immunostaining assay in cortical cultures. Neurons were transfected with a GFP-tagged NR2B subunit (the GFP tag is placed at the extracellular N terminus of NR2B). The GFP-NR2B has been shown to exhibit similar properties and localization as endogenous NR2B subunit (25). Surface distribution of the recombinant NR2B was assessed by immunostaining with anti-GFP primary antibody followed by rhodamine-conjugated secondary antibody in nonpermeabilized conditions.

Punctate red fluorescence was clearly visible on dendritic branches of the GFP-NR2B transfected cells under control conditions (Fig. 8*A*), whereas in neurons treated with nocodazole (30 μM, 40 min), the fluorescent GFP-NR2B surface clusters on dendrites were markedly reduced (Fig. 8*B*). The microtubule stabilizer taxol (10 μM, 15-min pretreatment) blocked the capability of nocodazole to reduce NR2B surface clusters on dendrites (Fig. 8*C*). Quantitative analyses (Fig. 8*D*) show that the surface NR2B cluster density on dendrites was significantly decreased by nocodazole (32.6 ± 0.7 clusters/30 μm in controls *versus* 19.0 ± 0.9 clusters/30 μm in nocodazole-treated neurons; $p < 0.01$, ANOVA), which was

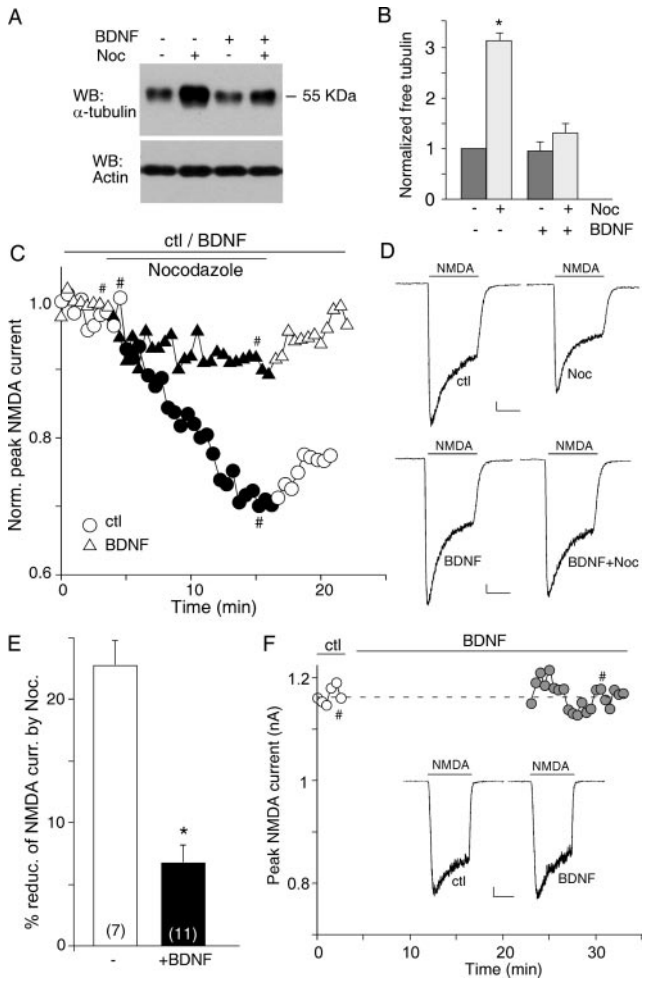

FIG. 7. **BDNF treatment blocked the microtubule depolymerizer-induced decrease of microtubule stability and suppression of NMDAR currents.** *A*, Western blot analysis of free tubulin in lysates of cultured PFC neurons treated without (−) or with nocodazole (*Noc*; 10 μM, 12 min) in the absence or presence of BDNF treatment (20 ng/ml, 60 min). Blotting (*WB*) of actin was used as a loading control. *B*, quantification of free tubulin assay. Free tubulin level was normalized to control (−), based on the intensity of the free tubulin band from Western blot analyses. *, $p < 0.001$, ANOVA. *C*, plot of normalized peak NMDAR currents showing the effect of nocodazole (30 μM) in the absence or presence of BDNF (10 ng/ml). *D*, representative current traces taken from the records used to construct *C* (at time points denoted by #). *Scale bars*, 100 pA, 1 s. *E*, cumulative data (mean ± S.E.) showing the percentage reduction of NMDAR currents by nocodazole in the absence or presence of BDNF. The number of cells tested is shown in *parentheses*. *, $p < 0.005$, ANOVA. *F*, plot of peak NMDAR currents showing the effect of BDNF (10 ng/ml) in a freshly dissociated PFC pyramidal neuron. *Inset*, representative current traces (at time points denoted by #). *Scale bars*, 100 pA, 1 s. *ctl*, control.

blocked by taxol (31.2 ± 1.3 clusters/30 μm in neurons treated with taxol *versus* 33.8 ± 1.0 clusters/30 μm in neurons treated with taxol + nocodazole). The average size of surface NR2B clusters on dendrites was also significantly decreased by nocodazole (0.33 ± 0.01 μm^2 in controls *versus* 0.16 ± 0.01 μm^2 in nocodazole-treated neurons; $p < 0.01$, ANOVA) (Fig. 8*D*), and this effect was blocked by taxol (0.32 ± 0.01 μm^2 in neurons treated with taxol *versus* 0.29 ± 0.01 μm^2 in neurons treated with taxol + nocodazole). The fluorescence intensity of surface NR2B clusters was largely unchanged (Fig. 8*D*). The total amount of NR2B receptor (GFP channel) was not altered by nocodazole treatment (data not shown). These data suggest that interfering with microtubule assembly reduces the number of surface NR2B subunits on neuronal dendrites.

DISCUSSION

In this study, we provide direct physiological evidence showing that the NMDAR response is regulated by microtubule dynamics. Agents that depolymerize microtubules cause a potent suppression of NMDAR-mediated currents. Unlike the actin regulation of NMDA channel activity (26), which occurs via Ca^{2+}/calmodulin-dependent release of NMDA receptors from the actin cytoskeleton (32), the microtubule regulation of NMDA channel activity is through a Ca^{2+}-independent process involving the motor protein-mediated dendritic transport of NR2B-containing NMDA receptors.

The trafficking of NMDA receptors has been an object of intense research effort recently, and most findings are concentrated in the subunit assembly, synaptic delivery, and internalization of NMDA receptors (2, 4, 7, 10). Much less is known about the dendritic transport of NMDA receptors before reaching synapses. Because microtubules are highly dynamic structures, undergoing rapid, GTP-dependent transitions between growth and shrinkage states (12), the regulatory effect of microtubule destabilizers could not be observed in GTP-free conditions (26). Moreover, our data suggest that only when a large pool of NMDA receptors on the membrane is activated by high concentrations of NMDA does the repression of microtubule-dependent transport of NMDA receptors on the dendrites have a significant impact on the NMDAR-mediated response.

The finding that KIF17, a member of the kinesin superfamily of microtubule motor proteins, indirectly associates with NR2B-containing vesicles (18) suggests that functional NMDA receptors on the plasma membrane can be regulated by microtubule-based transport (19). About 45 members of the kinesin protein superfamily (KIF proteins) have been identified, and they participate in selective transport of different cargoes to specific destinations in a microtubule- and ATP-dependent manner (33). The earlier identified KIF5 (originally called kinesin I) transports α-amino-3-hydroxy-5-methyl-4-isoxazolepropionic acid receptor-containing vesicles (34), and it has been found that the α-amino-3-hydroxy-5-methyl-4-isoxazolepropionic acid receptor-mediated, but not the NMDA receptor-mediated, transmission is affected by injection with an antibody against the kinesin I heavy chain (35). KIF17 transports NMDA receptor-containing vesicles by interacting through the LIN complex (18) and delivers at least 30% of NR2B in dendrites (19). Our present data show that specific suppression of KIF17 expression with antisense treatment prevents the regulation of NMDAR currents by interfering with microtubule dynamics, suggesting that the KIF17-mediated transport of NMDA receptors along microtubules plays an important role in the cellular response to NMDA.

In addition to motor proteins, another class of microtubule-binding proteins, such as microtubule-associated proteins (MAPs), can also modulate polymerization and stability of microtubules (36, 37). MAP2, a particular family of MAPs that is highly expressed in neuronal dendrites (38, 39), is an excellent *in vitro* substrate for several protein kinases (40). Phosphorylation of MAP2 affects the ability of MAP2 to bind and stabilize microtubules (41, 42). Neurotrophins, such as BDNF, prevent the destabilization of microtubule network and suppression of NMDAR currents by microtubule depolymerizers. One possible mechanism underlying this event is that BDNF treatment changes the phosphorylation state of MAP2, therefore altering the association of MAP2 with microtubules and subsequent microtubule stability (43, 44), leading to the change of microtubule-dependent transport of NMDA receptors.

To provide more direct evidence on the changes in the distribution of NMDARs in response to microtubule depolymerization, we performed surface labeling of GFP-tagged NR2B subunits

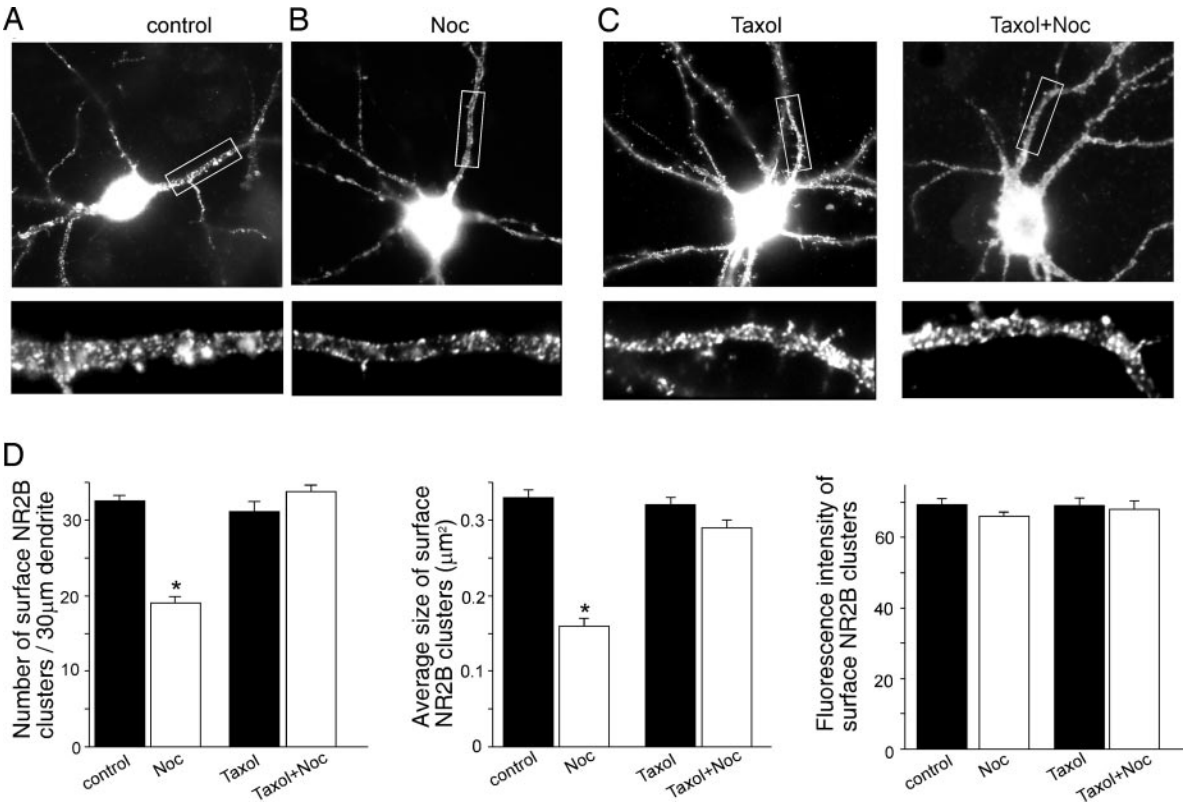

FIG. 8. **Microtubule depolymerizer treatment decreases the number of surface NR2B clusters on dendrites.** *A–C*, immunocytochemical images of surface NR2B in transfected cortical cultures treated without (*ctl*) or with nocodazole (*Noc*; 30 μM, 40 min) in the absence or presence of taxol (10 μM). Enlarged versions of the *boxed regions* of dendrites are shown *under* each of the *images*. *D*, quantitative analysis of surface NR2B clusters (cluster density, cluster size, and cluster intensity) along dendrites under different treatment. *, $p < 0.01$, ANOVA.

(25) in transfected cortical neurons. Microtubule depolymerizers significantly decreased the density and size of surface NR2B clusters on dendritic shafts, an effect blocked by the microtubule stabilizer taxol. These immunocytochemical results further prove that the inhibitory effect of microtubule depolymerizers on NMDAR currents is probably due to the reduction of the transport of NMDA receptors to dendritic membrane.

Taken together, this study shows that NMDAR function is regulated by microtubule dynamics. Emerging evidence has suggested that neurons require microtubule-based transport systems to ferry vital cellular cargoes to support their functions (45). Thus, the microtubule/kinesin-based transport system that is responsible for NMDA receptor trafficking provides a potentially important mechanism for regulating synaptic plasticity and associated learning and memory.

Acknowledgment—We thank Xiaoqing Chen for technical support.

REFERENCES

1. Carroll, R. C., and Zukin, R. S. (2002) *Trends Neurosci.* **25,** 571–577
2. Wenthold, R. J., Prybylowski, K., Standley, S., Sans, N., and Petralia, R. S. (2003) *Annu. Rev. Pharmacol. Toxicol.* **43,** 335–358
3. Petralia, R. S., Yokotani, N., and Wenthold, R. J. (1994) *J. Neurosci.* **14,** 667–696
4. Standley, S., Roche, K. W., McCallum, J., Sans, N., and Wenthold, R. J. (2000) *Neuron* **28,** 887–898
5. Scott, D. B., Blanpied, T. A., Swanson, G. T., Zhang, C., and Ehlers, M. D. (2001) *J. Neurosci.* **21,** 3063–3072
6. Washbourne, P., Bennett, J. E., and McAllister, A. K. (2002) *Nat. Neurosci.* **5,** 751–759
7. Roche, K. W., Standley, S., McCallum, J., Dune, L. C., Ehlers, M. D., and Wenthold, R. J. (2001) *Nat. Neurosci.* **4,** 794–802
8. Tovar, K. R., and Westbrook, G. L. (2002) *Neuron* **34,** 255–264
9. Lin, Y., Skeberdis, V. A., Francesconi, A., Bennett, M. V., and Zukin, R. S. (2004) *J. Neurosci.* **24,** 10138–10148
10. Vissel, B., Krupp, J. J., Heinemann, S. F., and Westbrook, G. L. (2001) *Nat. Neurosci.* **4,** 587–596
11. Lavezzari, G., McCallum, J., Dewey, C. M., and Roche, K. W. (2004) *J. Neurosci.* **24,** 6383–6391
12. Cleveland, D. W. (1982) *Cell* **28,** 689–691
13. Hirokawa, N. (1998) *Science* **279,** 519–526
14. Mitchison, T., and Kirschner, M. (1988) *Neuron* **1,** 761–772
15. Vaillant, A. R., Zanassi, P., Walsh, G. S., Aumont, A., Alonso, A., and Miller, F. D. (2002) *Neuron* **34,** 985–998
16. van Rossum, D., Kuhse, J., and Betz, H. (1999) *J. Neurochem.* **72,** 962–973
17. Goldstein, L. S., and Yang, Z. (2000) *Annu. Rev. Neurosci.* **23,** 9–71
18. Setou, M., Nakagawa, T., Seog, D. H., and Hirokawa, N. (2000) *Science* **288,** 1796–1802
19. Guillaud, L., Setou, M., and Hirokawa, N. (2003) *J. Neurosci.* **23,** 131–140
20. Feng, J., Cai, X., Zhao, J. H., and Yan, Z. (2001) *J. Neurosci.* **21,** 6502–6511
21. Chen, G., Greengard, P., and Yan, Z. (2004) *Proc. Natl. Acad. Sci. U. S. A.* **101,** 2596–2600
22. Wang, X., Zhong, P., Gu, Z., and Yan, Z. (2003) *J. Neurosci.* **23,** 9852–9861
23. Tyszkiewicz, J. P., Gu, Z., Wang, X., Cai, X., and Yan, Z. (2004) *J. Physiol.* **554,** 765–777
24. Joshi, H., and Cleveland, D. W. (1989) *J. Cell Biol.* **109,** 663–673
25. Luo, J. H., Fu, Z. Y., Losi, G., Kim, B. G., Prybylowski, K., Vissel, B., and Vicini, S. (2002) *Neuropharmacology* **42,** 306–318
26. Rosenmund, C., and Westbrook, G. L. (1993) *Neuron* **10,** 805–814
27. Vicini, S., Wang, J. F., Li, J. H., Zhu, W. J., Wang, Y. H., Luo, J. H., Wolfe, B. B., and Grayson, D. R. (1998) *J. Neurophysiol.* **79,** 555–566
28. Cull-Candy, S., Brickley, S., and Farrant, M (2001) *Curr. Opin. Neurobiol.* **11,** 327–335
29. Li, J. H., Wang, Y. H., Wolfe, B. B., Krueger, K. E., Corsi, L., Stocca, G., and Vicini, S. (1998) *Eur. J. Neurosci.* **10,** 1704–1715
30. Tovar, K. R., and Westbrook, G. L. (1999) *J. Neurosci.* **19,** 4180–4188
31. Williams, K. (1993) *Mol. Pharmacol.* **44,** 851–859
32. Zhang, S., Ehlers, M. D., Bernhardt, J. P., Su, C. T., and Huganir, R. L. (1998) *Neuron* **21,** 443–453
33. Hirokawa, N., and Takemura, R. (2005) *Nat. Rev. Neurosci.* **6,** 201–214
34. Setou, M., Seog, D. H., Tanaka, Y., Kanai, Y., Takei, Y., Kawagishi, M., and Hirokawa, N. (2002) *Nature* **417,** 83–87
35. Kim, C. H., and Lisman, J. E. (2001) *J. Neurosci.* **21,** 4188–4194
36. Hirokawa, N. (1994) *Curr. Opin. Cell Biol.* **6,** 74–81
37. Mandelkow, E., and Mandelkow, E. M. (1995) *Curr. Opin. Cell Biol.* **7,** 72–81
38. Bernhardt, R., and Matus, A. (1984) *J. Comp. Neurol.* **226,** 203–221
39. Caceres, A., Binder, L. I., Payne, M. R., Bender, P., Rebhun, L., and Steward, O. (1984) *J. Neurosci.* **4,** 394–410
40. Sanchez, C., Diaz-Nido, J., and Avila, J. (2000) *Prog. Neurobiol.* **61,** 133–168
41. Brugg, B., and Matus, A. (1991) *J. Cell Biol.* **114,** 735–743
42. Itoh, T. J., Hisanaga, S., Hosoi, T., Kishimoto, T., and Hotani, H. (1997) *Biochemistry* **36,** 12574–12582
43. Kowalski, R. J., and Williams, R. C., Jr. (1993) *J. Biol. Chem.* **268,** 9847–9855
44. Dhamodharan, R., and Wadsworth, P. (1995) *J. Cell Sci.* **108,** 1679–1689
45. Goldstein, L. S. (2003) *Neuron* **40,** 415–425